Graphene-based passively mode-locked bidirectional fiber ring laser

Venkatesh Mamidala,[1] R. I. Woodward,[2] Y. Yang,[1] H. H. Liu,[1] and K. K. Chow[1,*]

[1]*School of Electrical and Electronic Engineering, Nanyang Technological University, 50 Nanyang Avenue, Singapore 639798*

[2]*Femtosecond Optics Group, Department of Physics, Imperial College London, London, SW7 2AZ, UK*

[*]*kkchow@ntu.edu.sg*

Abstract: We present an all-fiber bidirectional passively mode-locked soliton laser with a graphene-based saturable absorber for the first time to the best of our knowledge. Our design includes a four-port circulator to introduce different sections of cavity for the two counter-propagating pulses, so they have distinct output characteristics. Simultaneous bidirectional operation is achieved by appropriately adjusting the net cavity birefringence and loss. In the clockwise direction, the laser emits ~750 fs pulses at 1561.6 nm, with a repetition rate of 7.68 MHz. In the counter clockwise direction, the central wavelength, pulse width, and repetition rate are 1561.0 nm, ~850 fs, and 6.90 MHz, respectively.

OCIS codes: (160.4330) Nonlinear optical materials; (060.3510) Lasers, fiber.

References and links

1. L. E. Nelson, D. J. Jones, K. Tamura, H. A. Haus, and E. P. Ippen, "Ultrashort-pulse fiber ring lasers," Appl. Phys. B **65**, 277-294 (1997).
2. M. E. Fermann, and I. Hartl, "Ultrafast fiber laser technology," IEEE J. Sel. Top. Quantum Electron. **15**, 191-206 (2009).
3. F. Dausinger, H. Lubatschowski, and F. Lichtner, *Femtosecond technology for technical and medical applications* (Springer, Berlin, 2004).
4. V. J. Matsas, T. P. Newson, D. J. Richardson, and D. N. Payne, "Self-starting passively mode-locked fiber ring soliton laser exploiting nonlinear polarization rotation," Electron. Lett. **28**, 1391-1393 (1992).
5. I. N. Duling, "All-fiber ring soliton laser mode-locked with a nonlinear mirror," Opt. Lett. **16**, 539-541 (1991).
6. O. Okhotnikov, A. Grudinin, and M. Pessa, "Ultra-fast fibre laser systems based on SESAM technology: New horizons and applications," New J. Phys. **6**, 177 (2004).
7. S. Y. Set, H. Yaguchi, Y. Tanaka, and M. Jablonski, "Ultrafast fiber pulsed lasers incorporating carbon nanotubes," IEEE J. Sel. Top. Quantum Electron. **10**, 137-146 (2004).
8. Q. L. Bao, H. Zhang, Y. Wang, Z. H. Ni, Y. L. Yan, Z. X. Shen, K. P. Loh, and D. Y. Tang, "Atomic-layer graphene as a saturable absorber for ultrafast pulsed lasers," Adv. Funct. Mater. **19**, 3077-3083 (2009).
9. Z. Sun, T. Hasan, F. Torrisi, D. Popa, G. Privitera, F. Wang, F. Bonaccorso, D. M. Basko, and A. C. Ferrari, "Graphene mode-locked ultrafast laser," ACS Nano **4**, 803-810 (2010).
10. A. Martinez, and S. Yamashita, "Carbon nanotube-based photonic devices: Applications in nonlinear optics", in *Carbon nanotubes applications on electron devices*, J. M. Marulanda, eds (InTech, 2011), pp. 367-386.
11. T. Hasan, Z. Sun, F. Wang, F. Bonaccorso, P. H. Tan, A. G. Rozhin, and A. C. Ferrari, "Nanotube-polymer composites for ultrafast photonics," Adv. Mater. **21**, 3874-3899 (2009).
12. X. Liu, D. Han, Z. Sun, C. Zeng, H. Lu, D. Mao, Y. Cui, and F. Wang, "Versatile multi-wavelength ultrafast fiber laser mode-locked by carbon nanotubes," Sci. Rep. **3**, 2718 (2013).
13. A. K. Geim, and K. S. Novoselov, "The rise of graphene," Nature Mater. **6**, 183-191 (2007).
14. F. Bonaccorso, Z. Sun, T. Hasan, and A. C. Ferrari, "Graphene photonics and optoelectronics," Nature Photon. **4**, 611-622 (2010).
15. Z. Sun, T. Hasan, and A. C. Ferrari, "Ultrafast lasers mode-locked by nanotubes and graphene," Physica E **44**, 1082-1091 (2012).
16. N. Buholz, and M. Chodorow, "3.2-Acoustic wave amplitude modulation of a multimode ring laser," IEEE J. Quantum Electron. **QE 3**, 454-459 (1967).
17. K. Kieu, and M. Mansuripur, "All-fiber bidirectional passively mode-locked ring laser," Opt. Lett. **33**, 64-66 (2008).

18. C. M. Ouyang, P. Shum, K. Wu, J. H. Wong, H. Q. Lam, and S. Aditya, "Bidirectional passively mode-locked soliton fiber laser with a four-port circulator," Opt. Lett. **36**, 2089-2091 (2011).
19. C. Zeng, X. Liu, and L. Yun, "Bidirectional fiber soliton laser mode-locked by single-wall carbon nanotubes," Opt. Express **21**, 18937-18942 (2013).
20. D. Mao, X. Liu, D. Han, and H. Lu, "Compact all-fiber laser delivering conventional and dissipative solitons," Opt. Lett. **38**, 3190-3193 (2013).
21. Y. Cui, and X. Liu, "Graphene and nanotube mode-locked fiber laser emitting dissipative and conventional solitons," Opt. Express **21**, 18969-18974 (2013).
22. Y. Hernandez, V. Nicolosi, M. Lotya, F. M. Blighe, Z. Y. Sun, S. De, I. T. McGovern, B. Holland, M. Byrne, Y. K. Gun'ko, J. J. Boland, P. Niraj, G. Duesberg, S. Krishnamurthy, R. Goodhue, J. Hutchison, V. Scardaci, A. C. Ferrari, and J. N. Coleman, "High-yield production of graphene by liquid-phase exfoliation of graphite," Nat. Nanotechnol. **3**, 563-568 (2008).
23. R. R. Nair, P. Blake, A. N. Grigorenko, K. S. Novoselov, T. J. Booth, T. Stauber, N. M. R. Peres, and A. K. Geim, "Fine structure constant defines visual transparency of graphene," Science **320**, 1308-1308 (2008).
24. A. C. Ferrari, J. C. Meyer, V. Scardaci, C. Casiraghi, M. Lazzeri, F. Mauri, S. Piscanec, D. Jiang, K. S. Novoselov, S. Roth, and A. K. Geim, "Raman spectrum of graphene and graphene layers," Phys. Rev. Lett. **97**, 187401 (2006).
25. M. A. Pimenta, G. Dresselhaus, M. S. Dresselhaus, L. G. Cancado, A. Jorio, and R. Saito, "Studying disorder in graphite-based systems by Raman spectroscopy," Phys. Chem. Chem. Phys. **9**, 1276-1291 (2007).
26. D. Von der Linde, "Characterization of noise in continuously operating mode-locked lasers," Appl. Phys., B Photophys. Laser Chem. **39**, 201-217 (1986).
27. C. Hönninger, R. Paschotta, F. Morier-Genoud, M. Moser, and U. Keller, "Q-switching stability limits of continuous-wave passive mode locking," J. Opt. Soc. Am. B **16**, 46-56 (1999).

1. Introduction

Passively mode-locked fiber lasers delivering ultra-short optical pulses have been extensively studied owing to their unique advantages including high peak power, excellent pulse stability, high power conversion efficiency, compact design, alignment-free nature, efficient heat dissipation, reliability, and low cost [1]. Such laser properties are sought for a wide range of scientific and technological applications such as high speed optical communications, material processing, supercontinuum generation, optical frequency metrology, biomedical applications, etc [2, 3].

To achieve passive mode-locking of a fiber laser, different techniques including nonlinear polarization rotation (NPR) [4], nonlinear amplifying loop mirrors (NALM) [5] and saturable absorbers (SA) [6, 7] have been used. Among these techniques, SA-based mode-locking is thought to be more efficient and environmentally stable. Widely used SAs to achieve mode-locking in fiber lasers are semiconductor saturable absorber mirrors (SESAMs) [6], carbon nanotubes (CNTs) [7], and recently graphene [8, 9]. Among them, SESAMs have been widely used for generating Q-switched and mode-locked laser pulses [6]. However, their complex fabrication and narrow operational wavelength range limits their practical applications [6]. As a simple alternative, CNTs have emerged as promising SAs because of their ultrafast recovery time, cost-effective production and ease of fiber integration [7, 10-12]. The bandgap of CNTs depends on the diameter and chirality of nanotubes [10]. A broadband SA is possible using CNTs with a wide diameter distribution [11]. However, only CNTs with a certain diameter contribute to the saturable absorption of a particular wavelength of light; the remaining tubes which are not in resonance give large non-saturable losses.

Recently, graphene, a two-dimensional atomic layer of carbon atoms, has proven to be a novel SA for the development of ultrafast lasers [8, 9]. The gapless linear dispersion of Dirac electrons allows broadband saturable absorption in graphene [13]. Additionally, graphene has the intrinsic advantages of an ultrafast recovery time, higher damage threshold, lower saturation intensity and the ability to operate in transmission, reflection, and bidirectional modes [14]. All of these factors make graphene an ideal SA for mode-locked lasers over an ultra-wide spectral range from the visible to the far-infrared. Graphene-based SAs are preferred over SESAMs and CNTs as they do not require band-gap design and diameter

control to improve their performance. Since the demonstration of the first fiber laser mode-locked by a graphene-based SA, a series of fiber and bulk lasers have been reported, emitting different wavelengths and pulse widths [15].

Typically, unidirectional ring configurations are widely adopted in passively mode-locked fiber lasers. An optical isolator is employed inside the cavity to reduce the spurious cavity reflections and decrease the self-starting mode-locking threshold. The isolator in a ring cavity enables only unidirectional operation. On the other hand, mode-locked fiber lasers without an optical isolator inside their cavities can simultaneously generate two pulse trains (bidirectional mode-locking), which are attractive devices for various sensing applications [16].

The first demonstration of a bidirectional mode-locked laser was given by *Buholz* and *Chodorow* [16], subsequently several groups have reported bidirectional mode-locked lasers based on different active media. Recently, *Kieu* and *Mansuripur* presented the first all-fiber bidirectional passively mode-locked ring laser at 1.55 μm [17]. To enable bidirectional mode locking in their laser, they used a fiber taper embedded in a CNT-polymer composite as an SA. In their experiments, the two counter propagating pulse trains exhibited very similar performance in terms of pulse duration, spectrum, and repetition rate. By using two SESAMs, *Ouyang et al.* reported a bidirectional passively mode-locked fiber laser at 1.56 μm [18]. In their work, much of the focus is on the different output properties of two counter-circulating pulse trains.

More recently, *Zeng et al.* demonstrated a bidirectional passively mode-locked erbium-doped fiber (EDF) laser with single-walled CNTs (SWNTs)-polyvinyl alcohol mode-locker [19]. By appropriately adjusting the polarization controller (PC) and designing the cavity, they achieved simultaneously two stable soliton pulse trains with the same or different central wavelengths. *Mao et al.* reported the simultaneous generation of conventional soliton (CS) and dissipative soliton (DS) in a mode-locked fiber laser by inserting a chirped fiber Bragg grating and a four-port circulator into the cavity [20]. *Cui* and *Liu* proposed a bidirectional passively-mode-locked fiber laser based on the mixture of graphene and SWNTs [21]. By adjusting intra-cavity loss and pump power, their laser can deliver two different types of pulses (DS and CS) in opposite directions. Unfortunately, they did not achieve simultaneous mode-locking operation in both directions.

In this paper, we report, for the first time to the best of our knowledge, a passively mode-locked bidirectional fiber laser with a graphene saturable absorber. Two stable soliton pulse trains with distinct output characteristics can be achieved simultaneously in clockwise (CW) and counterclockwise (CCW) directions. Our proposed cavity includes a shared main-path and two sub-paths. Because of this unique design, the properties of the counter-circulating pulse trains could be varied independently by altering the sub-path parameters (such as the dispersion, fiber length and saturable absorber), providing two femtosecond pulse trains with distinct and variable properties. The laser can also be used as a test-bed for saturable absorbers.

2. Preparation of the graphene-based SA and characterization

Kish Graphite flakes purchased from Graphene Supermarket were used to prepare the few layer graphene. The graphite flakes were exfoliated for 12 hours by ultrasonication in N,N-Dimethylformamide (DMF) then kept aside overnight to precipitate the unexfoliated graphitic particles [22]. The resulting graphene dispersion is then centrifuged at 4500 rpm for 1 hour at room temperature to remove any large aggregates. High quality graphene dispersions were obtained by collecting the supernatant from the centrifuged samples which was predominantly composed of sub-micrometer graphene flakes. The dispersions were stable against sedimentation and displayed no further aggregation for a period of weeks.

To prepare our graphene-based SA, we adopted the conventional approach in which dispersions of graphene were sprayed onto a fiber patch cord end facet (or fiber ferrule) with N_2 gas [10]. We confirmed that no droplets were formed on the end facet of the fiber patch

cord during spraying, which resulted in deposition of graphene and the formation of a homogeneous graphene layer. The total insertion loss of the graphene based SA is about 2±0.2 dB.

A UV-visible absorption spectrum was measured on a Perkin-Elmer Lambda 950 spectrophotometer. The centrifuged dispersions were diluted and drop-cast onto a Si wafer with 300 nm thermally grown SiO_2. The drops were dried at room temperature. These samples were then used for Raman measurements, collected with a WITec Raman microscope at 532 nm excitation. The spot size of the laser beam was about 1 μm in diameter using a 100× objective lens. Using the same samples, scanning electron microscopy (SEM) images of graphene flakes were taken with a standard SEM system (JEOL JSM-5900LV).

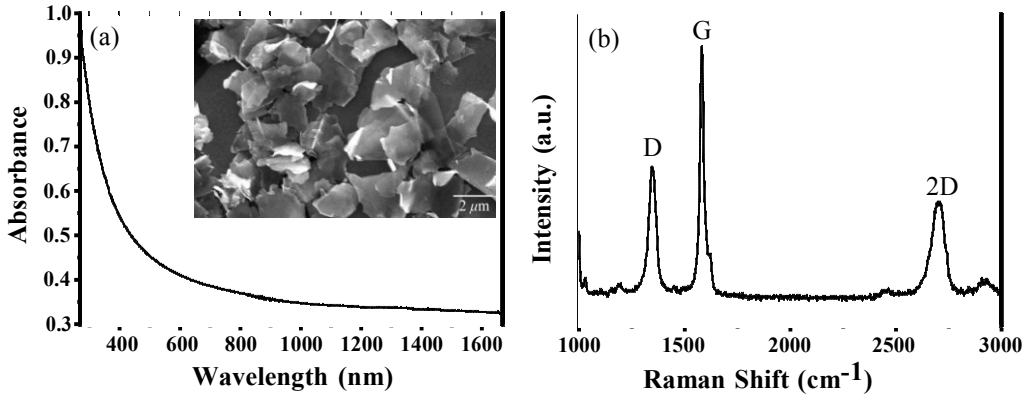

Fig. 1. (a) Absorption spectrum of 20% diluted graphene solution. The inset shows an SEM image of graphene flakes. (b) Raman spectra of graphene flakes.

Figure 1(a) plots the absorption spectra of graphene flakes dispersed in DMF solution. As expected, it was flat and featureless over a wide spectral range [22, 23]. The inset of Fig. 1(a) shows the SEM image of graphene flakes. Figure 1(b) shows the Raman spectrum of the graphene flakes with three characteristic peaks D (~1344 cm^{-1}), G (~1581 cm^{-1}), and 2D (~2703 cm^{-1}). The broader linewidth of the 2D-band represents the characteristic of few layer graphene flakes [24]. The disorder-related D peak is a result of defects within the graphene sheets or from the small size of the flakes, which would increase the number of disordered graphene edges. The low ratio of the intensities of the D and G peaks [I(D)/I(G) ~ 0.95] implies that as-produced graphene flakes possesses a small number of structural defects [25].

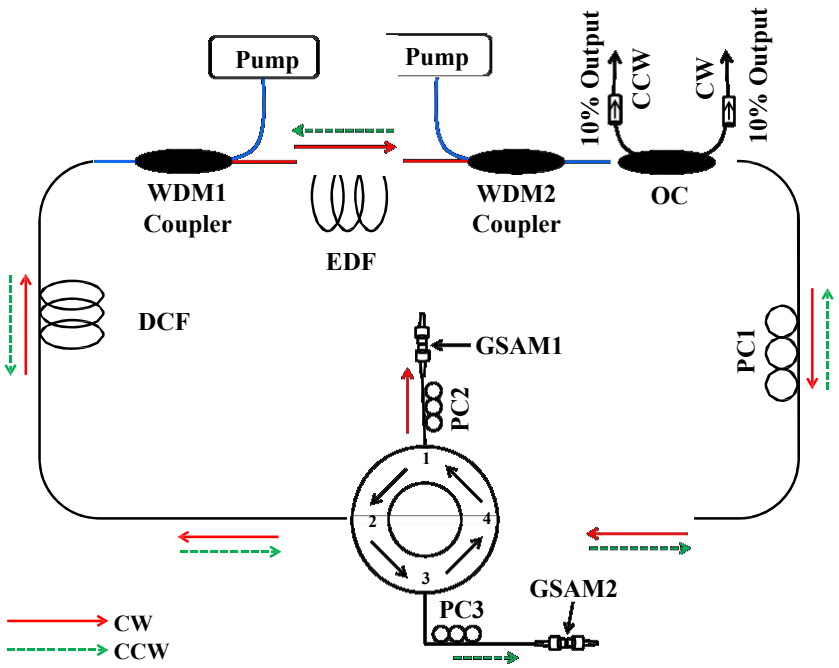

Fig. 2. Experimental setup of the bidirectional fiber laser. WDM, wavelength-division multiplexer; EDF, erbium-doped fiber; CW, clockwise; CCW, counterclockwise; OC, output coupler; DCF, dispersion compensating fiber; PC, polarization controller; GSAM, combination of graphene-based SA with fiber mirror.

We investigated the saturable absorption properties of our graphene-based SA using power-dependent transmission measurement. A home-built mode-locked laser was used as a pulse source, operating at 1561.5 nm, with a pulse width of 390 fs and repetition rate of 68.8 MHz. The saturable and non-saturable absorption components were estimated to be ~2% and ~40%, respectively.

3. Experimental setup

The experimental setup of the graphene-based passively mode-locked bidirectional fiber laser is as shown in Fig. 2. A 60 cm long EDF (nLight LIEKKI Er110-4/125) with group velocity dispersion (GVD) of 0.012 ps^2/m and a peak core absorption of 110 dB/m at 1530 nm was used as the gain medium. The laser was pumped (either unidirectionally or bidirectionally) with a 974 nm laser by the use of fused 980/1550 nm wavelength division multiplexer (WDM) coupler. The pump laser has a maximum output power of 300 mW.

As shown in Fig. 2, our laser ring cavity consists of a shared main-path and two different sub-paths between the four-port circulator. The polarization-dependent four-port circulator facilitates the bidirectional operation, in which the light propagates from the ports 1→2, 2→3, 3→4, and 4→1. The main-path is made of two WDM couplers, a 2×2 10/90 output coupler (OC), polarization controller (PC) and dispersion compensating fiber (DCF) (GVD of -6×10^{-4} ps^2/m) and the two sub-paths consist of a PC and a graphene based SA which is mated to a highly reflective fiber mirror. The combination of a graphene based SA and fiber mirror serves as a reflective SA, here we call the combination a Graphene Saturable Absorber Mirror (GSAM). The main-path and sub-paths are connected by ports (4→1 or 2→3) of the circulator, which enables mode-locking of light propagating in both CW and CCW directions. The OC in the cavity extracts 10% of the power in each direction. External to the cavity, two

polarization-independent isolators are used to exclude the reflection from the output fiber ends.

The main-path has a length of ~17.5 m, which includes single mode fiber (SMF) pigtails, polarization-maintaining (PM) fiber pigtails from port 2 and 4 of circulator, 3 m of DCF in PC1 and 9.5 m of DCF. Sub-paths have a length of 4.3 m and 5.7 m, which includes different lengths (3 and 4 m) of SMF in PC and SMF pigtails. In CW direction, light propagates from EDF→OC→PC1→Port4→Port1→PC2→GSAM1→PC2→Port1→Port2→DCF. The net dispersion and length of cavity are about -0.29 ps^2 and ~26 m, respectively. On the other hand, in CCW direction light propagates from EDF→DCF→Port2→Port3→PC3→GSAM2→PC3 →Port3→Port4→PC1→OC. In this direction, the net dispersion and length of cavity are about -0.36 ps^2 and ~29 m, respectively. The counter-circulating pulses always share the main-path but they face a different GSAM in their sub-paths. Since the fiber laser operates in the net-anomalous dispersion regime, soliton shaping is enabled in both directions. However, the temporal and spectral properties of the output pulses in each direction can be different as they travel in different sub-paths and experience effects in the cavity such as gain and loss in a different order. PC1 is used to adjust the net birefringence of the cavity. Bidirectional operation of the CW and CCW pulses can be achieved by introducing controllable losses through adjusting the PC between the circulator and GSAM. In our cavity, the circulator is polarization-maintaining which blocks the fast axis. So, the combination of PC2 (or PC3) and the circulator act as a tunable attenuator.

The performance of the bidirectional laser was simultaneously monitored using two optical spectrum analyzers (Ando), 2 GHz photodetector (Thorlabs DET01CFC) followed by a 350 MHz oscilloscope (Agilent Technologies), signal source analyzer (Rohde & Schwarz FSUP26) and an optical autocorrelator (Alnair Labs HAC-200).

4. Results and Discussion

In the experiment, first we used unidirectional pumping by using WDM1. When the pump power was ~175 mW, self-starting mode-locked laser operation was observed in the CCW direction. This mode-locking priority is partially because of the different cavity losses faced by light in CW and CCW directions. For example, in the CW direction, light propagates through the OC before the GSAM, resulting in 10% less power incident on the GSAM compared to the light propagating in the CCW direction. In order to achieve bidirectional mode-locking operation, it is necessary to impose an extra loss on the CCW-propagating pulse train to balance the effective net gain of the counter-circulating light within the cavity. By adjusting all three PC's, we can obtain simultaneous mode-locking in both directions. We noticed that adjusting only PC1 helps to vary the net birefringence of the cavity but it does not help to achieve simultaneous mode-locking. By changing PC2 and PC3, we introduced additional loss in the CCW direction that provides sufficient net gain for both directions. At this stage, the laser produces multiple pulses within a round-trip time. By carefully reducing the pump power to 150 mW, we can achieve single pulse soliton operation in both directions. Once simultaneous mode-locking was initiated, the pulse trains could be very stable for many hours.

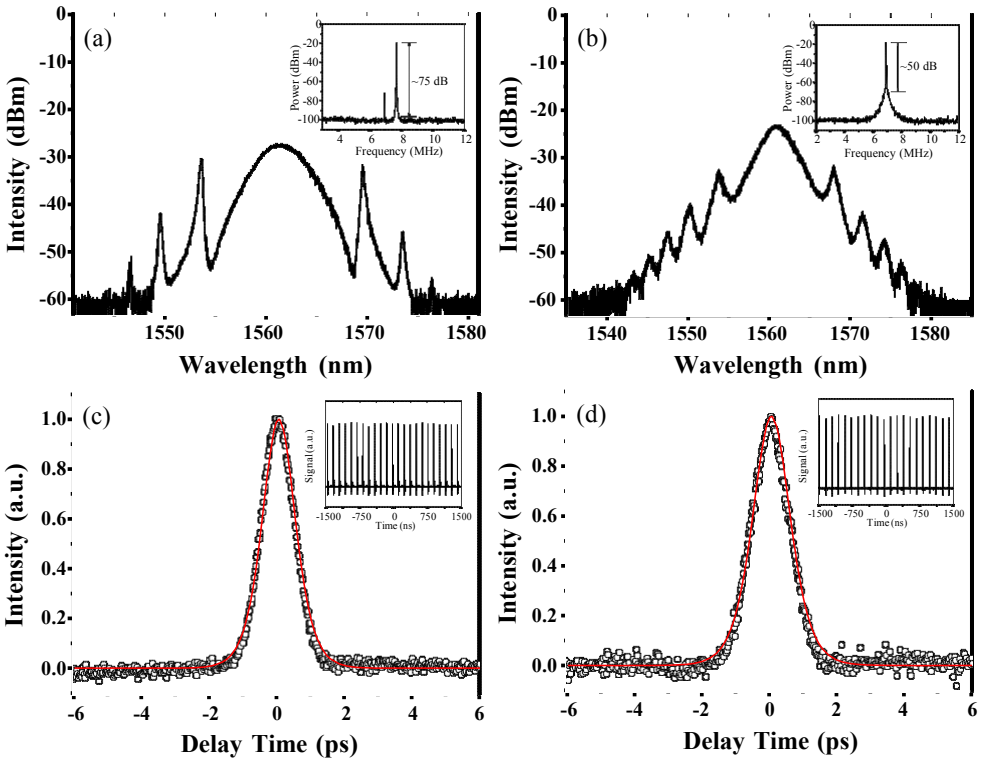

Fig. 3. Unidirectional pumping: Output optical spectrum of the CW pulses (a) and the CCW pulses (b). Insets are the corresponding RF spectra. Autocorrelation traces of the CW pulses (c) and the CCW pulses (d). Insets are the oscilloscope traces.

Figures 3(a) and 3(b) show the laser output spectrum of the counter-circulating pulse trains with resolution bandwidth of 0.02 nm. The spectrum was centered at 1561.6 nm for CW and 1561.0 nm for CCW directions. The full width at half maximum (FWHM) bandwidths of the two spectra are 4.2 nm and 3.2 nm, respectively. Since both directions have net-anomalous dispersion the generated pulse spectra have a soliton-like shape with characteristic Kelly sidebands. The inset of Fig. 3(a) and 3(b) illustrate the radio frequency (RF) spectrum of the simultaneously mode-locked laser measured with 1 kHz resolution bandwidth and 10 MHz span. The fundamental repetition rate of the CW pulse train was ~7.68 MHz and ~6.90 MHz for the CCW direction. The peak at ~6.90 MHz in the RF spectrum of the CW direction is due to a small reflection of light from the CCW pulse train. We verified this by removing GSAM2 to suppress CCW lasing and noted that this peak disappeared. The peak-to-pedestal ratio of the RF spectrum for CW-propagating pulses was ~75 dB, implying good mode-locking stability [26]. A lower ratio of ~50 dB was observed for the CCW direction, suggesting that this mode-locked pulse train is slightly noisier, which could be related to the different sub-paths in CW and CCW directions and the order of components experienced by light in the cavity, in addition to the different output powers.

The pulse shapes were investigated using an autocorrelator and the corresponding traces together with a sech^2 fit are reported in Fig. 3(c) and 3(d). The corresponding pulse durations of the CW and CCW pulses were ~750 fs and ~850 fs, respectively. The time-bandwidth products (TBP) of the counter-circulating pulses were calculated as 0.39 and 0.34, indicating that the output pulses were nearly transform-limited soliton pulses. As depicted in the insets of Fig. 3(c) and 3(d), the fundamental repetition rates for counter-circulating mode-locked pulses

were not identical because of their distinct cavity lengths. The corresponding repetition rates for CW and CCW directions were measured as ~7.68 MHz and ~6.90 MHz. By observing the pulse trains over a long range, we notice only very minimal Q-switching instabilities in the mode-locking regime. Q-switching instabilities can arise due to interplay between saturation effects in the SA, and the gain medium favoring higher pulse energies with lower round trip losses [27]. We believe the slight instability we observe is due to the low modulation depth (~2%) and high non-saturable loss (~40%) of the SA, which is a cause of the noise we observe in the optical and RF spectra. Fabrication of a graphene SA with higher modulation depth is expected to reduce this instability and improve mode-locking performance. We also expect our cavity design will enable bidirectional mode-locking at other wavelengths if appropriate gain fiber and couplers are used, since graphene is an ultra-wideband SA.

Under an incident pump power of 150 mW, the average output power for the CW and CCW directions was 180 μW and 400 μW, respectively. The calculated pulse energy was 23.5 pJ and 58 pJ, respectively. Asymmetry of the laser cavity is the reason behind the different average output powers.

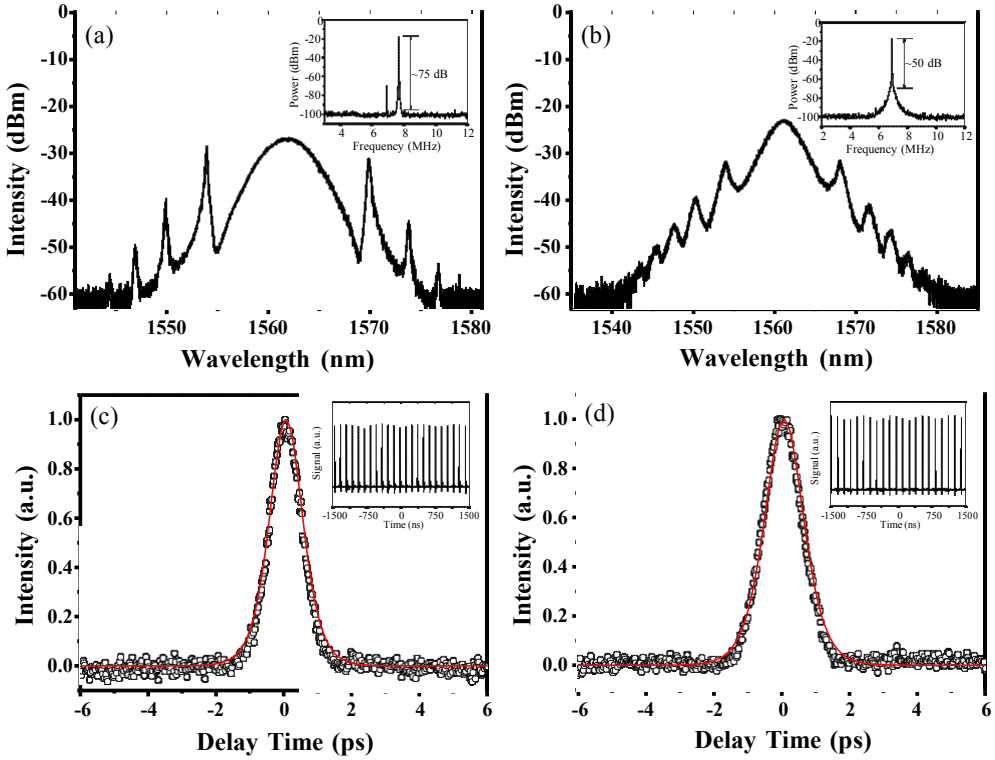

Fig. 4. Bidirectional pumping: Output optical spectrum of the CW pulses (a) and the CCW pulses (b). Insets are the corresponding RF spectra. Autocorrelation traces of the CW pulses (c) and the CCW pulses (d). Insets are the oscilloscope traces.

Subsequently, we used bidirectional pumping by using both WDMs. Similar to unidirectional pumping, mode-locking of the laser self-started in CCW direction at a pump power of ~200 mW (with forward pump power of 120 mW and backward pump power of 80 mW). In order to initiate simultaneous mode-locking, careful adjustment of PC1, PC2 and PC3 was required. At first, multiple pulses were observed in each round-trip of the cavity, then by reducing the pump power to 175 mW (with forward pump power reducing to 95 mW and the backward pump power reducing to 80 mW) we were able to achieve fundamentally

mode-locked single pulse soliton operation in both directions. Once simultaneously mode-locked, the laser would remain stable for hours.

The output optical spectra of the simultaneously generated CW and CCW light pulses are shown in Fig. 4(a) and 4(b). The central wavelengths of the CW and CCW pulses were located at 1561.9 nm and 1561.1 nm, respectively. The FWHM spectral bandwidth for the CW direction was 4.4 nm and 3.4 nm for the CCW direction. The counter-circulating pulses exhibit spectral sidebands, which clearly indicate soliton pulse shaping. The RF spectrum of laser is shown in the inset of Fig. 4(a) and 4(b), indicating a repetition rate of ~7.68 MHz for CW-propagating light and ~6.90 MHz for the CCW pulse train. The measured peak-to-pedestal ratio for the CW and CCW directions was ~75 dB and ~50 dB, respectively.

Figures 4(c) and 4(d) illustrate the measured autocorrelation traces for both directions including a sech^2 fit, which indicates a width of ~750 fs and ~880 fs for CW and CCW pulses respectively. Taking into account spectral bandwidths, the TBP of the laser is equal to 0.41 and 0.37, which is close to the transform limit for sech^2-shaped laser pulses. Insets of Fig. 4(c) and 4(d) show the measured oscilloscope trace of the output mode-locked pulses. The counter-circulating pulses operate at a period of 130 ns and 145 ns. The average output power of CW and CCW soliton pulses was about 200 μW and 430 μW, corresponding to pulse energies of 26 pJ and 62 pJ.

The mode-locked pulse train characteristics are very similar for our laser when using either a unidirectional or bidirectional pump scheme. This shows that despite the bidirectional propagation of pulses in our laser cavity, the choice of pumping a single end of the gain medium or pumping both ends does not have a significant effect on the performance of our laser.

5. Conclusion

In conclusion, we have reported a graphene-based passively mode-locked bidirectional fiber laser. Two counter-circulating trains of soliton pulses with distinct output characteristics were generated simultaneously. This was achieved by appropriately adjusting the cavity birefringence and introducing controllable losses through the combination of a fast-axis blocking PM circulator and PC. The unique features offered by bidirectional mode-locked fiber lasers, along with the easy graphene SA preparation pave the way to dual ultrafast light sources in a single simple low-cost cavity.

Acknowledgments

The authors would like to acknowledge Dr. K. Wu for providing the fiber mirrors. This work was partially supported by Academic Research Fund Tier 1 Grant (RG22/10) of Ministry of Education and Nanyang Technological University, Singapore.